Characterization of Ambipolar GaSb/InAs Core–Shell Nanowires by Thermovoltage Measurements

Jan G. Gluschke,[*,†,‡] **Martin Leijnse,**[†] **Bahram Ganjipour,**[†] **Kimberly A. Dick,**[†,§] **Heiner Linke,**[†] **and Claes Thelander**[*,†]

[†]Solid State Physics and Nanometer Structure Consortium (nmC@LU), Lund University, Box 118, S-22100 Lund, Sweden, [‡]School of Physics, The University of New South Wales, Sydney, New South Wales 2052, Australia, and [§]Center for Analysis and Synthesis, Lund University, Box 124, S-22100 Lund, Sweden

ABSTRACT In semiconductor heterostructures with a type II band alignment, such as GaSb–InAs, conduction can be tuned from electron- to hole-dominated using an electrostatic gate. However, traditional conductance measurements give no direct information on the carrier type, and thus limit the ability to distinguish transport effects originating from the two materials. Here, we employ thermovoltage measurements to GaSb/InAs core–shell nanowires, and reliably identify the dominant carrier type at room temperature as well as in the quantum transport regime at 4.2 K, even in cases where the conductance measurement does not allow for such a distinction. In addition, we show that theoretical modeling using the conductance data as input can reproduce the measured thermovoltage under the assumption that electron and hole states shift differently in energy with the applied gate voltage.

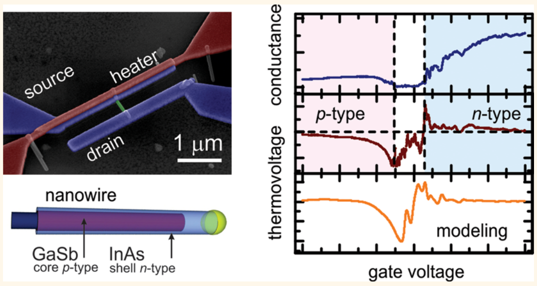

KEYWORDS: thermovoltage · core/shell · nanowires · field effect · ambipolar · GaSb/InAs

Heterostructures of GaSb and InAs show an uncommon type II-broken gap band alignment,[1] which is tunable by confinement,[2] and of relevance to a wide range of topics, such as tunnelling-based devices,[3−6] far-infrared detectors,[7,8] and research on electron–hole hybridization.[9,10] Recently, this heterostructure has been realized in a novel core–shell geometry through growth of nanowires,[11] and studied by conductance measurements.[6,12] The nanowires were found to exhibit tunable, ambipolar conductivity, attributed to holes in the GaSb core, and electrons in the InAs shell.[13]

However, a major limitation in the development of these structures is that many standard methods to extract information on carrier type, density, and mobility, such as Hall measurements,[14] cannot be applied due to the complicated core–shell geometry and nearly 1D structure of nanowires. Due to such limitations, thermoelectric measurements are currently being established as a complementary tool to electrical measurements to estimate carrier mobility[15,16] and concentration,[16] relaxation time,[16] and Fermi-level position[17] in various nanostructures, as well as to investigate various quantum-transport phenomena.[18−25]

Characterization of ambipolar nanostructures poses additional challenges, such as determining the relative contribution of each carrier type to the transport as a function of Fermi-level position. For gated structures, it is also important to separately determine the gate lever arm that describes how the electron and hole states shift in energy when a gate voltage is applied. Standard conductance measurements do not yield information regarding either of these points.

In this work, we show that thermovoltage measurements, due to their sensitivity to charge carrier type,[26] are a powerful tool for the study of ambipolar transport. Applying the technique to GaSb/InAs core–shell nanowires, we determine the dominant carrier type in different transport regimes, including that of single charge tunneling. More specifically, we present conductance (G) and thermovoltage (V_{Th}) measurements

* Address correspondence to
jan.gluschke@nanoelectronics.physics.unsw.edu.au,
claes.thelander@ftf.lth.se.

Received for review March 9, 2015
and accepted June 19, 2015.

10.1021/acsnano.5b01495

at temperatures between 4.2 and 295 K as a function of back-gate voltage V_g. A clear sign change in the thermovoltage is observed with increasing V_g, which supports the interpretation of a crossover in charge transport from hole conduction in the core, to electron conduction in the shell. Even in cases where $G(V_g)$ increases monotonically and does not show any sign of ambipolar conduction, which is often the case at room-temperature, complementary thermovoltage measurements still show clear evidence of a hole contribution to the transport.

At 4.2 K, thermovoltage measurements are also used to determine the dominant carrier type involved in conductance resonances observed in a regime where both core and shell are nearly depleted. We assign these resonances to 0D states induced by potential disorder at the nanowire surface, an interpretation that is supported by the observation of nonlinear thermovoltage effects from the application of large thermal gradients in the electron regime.

Finally, we show that the measured thermovoltage data can be reproduced by a simple transport model using the conductance measurements as input, if $G(V_g)$ is divided into two intervals where the transport is dominated by electrons and holes, respectively. To reach good qualitative agreement with the measured V_{Th}, we further need to assume that hole states in the regime of hole conduction have a weaker shift with applied gate voltage than corresponding electron states in the electron conduction regime. Gaining insight into the relative shift in the electron and hole states with V_g is important for understanding transport in ambipolar structures in general, and specifically in recent complex bipolar heterostructure devices, such as tunnel transistors.[27]

DEVICE AND THEORETICAL BACKGROUND

Device. Figure 1a displays a scanning electron microscopy (SEM) image of a representative device used in this study. It features two electrical contacts (blue) to the nanowire (green) and a microstrip heater line (red) that runs on top of one contact, but is electrically insulated from it with a thin HfO_2 film. To introduce a temperature gradient ΔT across the nanowire, a heating voltage V_H is applied over the heater line with resistance R_H inducing a heating current I_H. The resulting Joule heat $Q \propto I_H{}^2 R_H$ elevates the temperature at the nanowire contact. The positioning of the heater directly on top of the contact allows for the application of temperature differences of several tens of Kelvin while not producing any measurable temperature increase of the contact on the cold side of the nanowire. A detailed analysis of this heating method is reported elsewhere.[28] The conductance $G = I_D/V_{SD}$ is measured using a constant dc source-drain voltage V_{SD} while measuring the drain current I_D. The highly doped Si substrate with a 100 nm SiO_2 layer was used as a back gate.

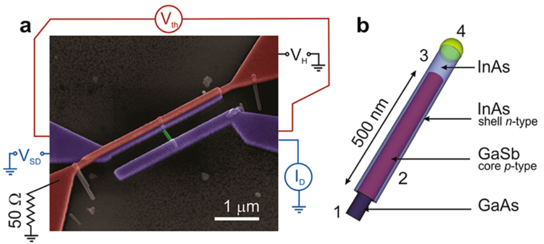

Figure 1. (a) Scanning electron micoscope (SEM) image of a typical device used for the thermoelectric (TE) characterization of a single GaSb/InAs core−shell nanowire. A heater (red) is placed directly on top of the ohmic source-drain contacts (blue) to the nanowire (green), electrically insulated by a 10 nm HfO_2 layer. This allows for the application of temperature differences of several tens of Kelvin along the approximately 500 nm long core−shell segment of the nanowire. (b) Schematic illustration of a GaSb/InAs core−shell nanowire. The core−shell segment (2) of the nanowire consists of a *p*-type GaSb core (approximately 70 nm in diameter) and a 5−7 nm thick *n*-type InAs shell. The axially adjacent InAs segment (3) has *n*-type transport characteristics, whereas the neighboring GaAs segment (1) is electrically insulating. The gold particle (4) serves as a catalyst during the growth process.

Figure 1b displays a schematic illustration of a GaSb/InAs core−shell nanowire. The wires consist of (1) a short axial GaAs segment involved in the nucleation of the nanowire, (2) an approximately 500 nm long GaSb/InAs core−shell segment, (3) an axial InAs segment which forms during the growth of the shell, and (4) the gold particle responsible for the nanowire growth. Due to an Sb memory effect in the growth reactor, the InAs in the shell as well as in the axial segment has a small background Sb incorporation, but for simplicity, we will refer to this material as InAs in the text. For this study, only the core−shell segment of the nanowire was intentionally contacted, and charge transport was studied along the nanowire length.

Theoretical Background. For the general interpretation of the measurement data, we assume that the transport in the core and shell occurs in two parallel, but separate, channels. Electron−hole interaction effects such as Coulomb drag are not considered. The conductance G of the investigated core−shell segment is then given by $G = G_e + G_h$, where G_e is the conduction due to electrons in the shell and G_h is the conductance due to holes in the core. The combined Seebeck coefficient S is given by,

$$S = \frac{S_e G_e + S_h G_h}{G_e + G_h} = \frac{G_e^T + G_h^T}{G_e + G_h} = -\frac{V_{Th}}{\Delta T} \quad (1)$$

where S_e and S_h denote the Seebeck coefficients corresponding to the two channels. G^T gives the ratio between a thermally driven current and ΔT in the absence of an electrical bias, $I_{Th} = G^T \Delta T$. The Seebeck coefficient for holes S_h is generally positive (negative V_{Th}) and S_e is negative (positive V_{Th}). A low-temperature approximation of the relationship between S and the conductance G is given by the Mott relation $S \sim (1/G(E))$

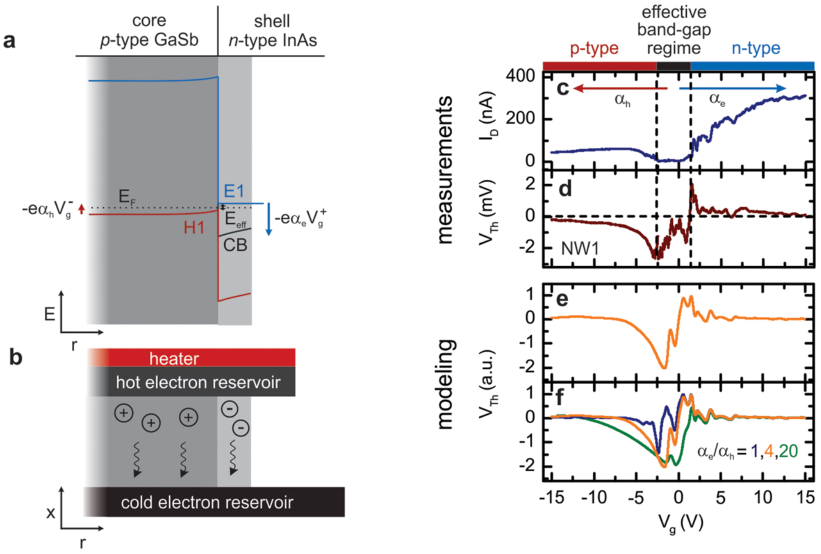

Figure 2. (a) Schematic illustration of the bandstructure at the interface between a *p*-type GaSb-core and an *n*-type InAs-shell segment. In the displayed configuration, the lowest electron-subband edge (E1) is elevated above the conductance band edge of InAs in bulk (CB). In fact, E1 is located above the first hole-subband (H1) of the GaSb forming a type II-staggered band alignment with an effective band gap E_{eff}. If the Fermi energy E_F is located in the effective band gap, both core and shell of the nanowire are pinched off and a zero-current plateau is observed in the conductance of nanowire NW1 (c). (b) Under the application of a thermal bias, holes in the core and the electrons in the shell diffuse from the hot to the cold end of the nanowire building up a thermovoltage V_{Th} under open circuit conditions (d). If a gate voltage V_g is applied, the subbands shift by $-e\alpha V_g$. For large positive gate voltages (V_g^+) the shell is populated with free electrons leading to an increase in conductance with V_g and a positive thermovoltage. In the case of a large negative gate voltage (V_g^-), the shell is pinched off and the core is populated with free holes leading to a decrease in conductance with V_g and negative thermovoltage. (e and f) The experimental thermovoltage data can be reproduced well using modeling based on the conductance data if the ratio of the gate lever arms α_e/α_h of core and shell is chosen so that the electron states in the shell couple 4 times stronger to the gate than the hole states in the core (orange trace). I_D was measured using a source-drain bias V_{SD} of 5 mV and the thermovoltage with a heating power P_H of 0.37 mW.

$dG(E)/dE\,|_{E=E_F}$, where E is energy and E_F is the Fermi energy. $G(E)$ can roughly be described as the conductance of electrons with energy E (it is the transmission function in the ballistic case[29] and the transport distribution function in the diffusive case[30,31]). A more in-depth discussion of the origin of the sign of S is provided in the Supporting Information (S1). In low-temperature transport studies, it is generally assumed that E is proportional to V_g, such that $S \sim (1/G)\, dG/dV_g$.[18,24,32] In this case, a measurement of $S(V_g)$ does not, in principle, reveal any additional information not contained in $G(V_g)$, but has the advantage of providing a large signal in regions with a very small conductance. However, in nanostructures with several small intrinsic energy scales, the Mott relation may not hold even at rather low measurement temperatures,[33] and $S(V_g)$ reveals information not contained in $G(V_g)$, for example about states at higher energies. In the case of heterostructures, such as the core–shell structures studied in this work, one cannot relate $G(E)$ and $G(V_g)$ if the different conductance channels do not equally couple to the gate.

RESULTS AND DISCUSSION

Basic Measurements and Modeling. The confinement-induced energy shift of the electron states in the InAs shell determines the band alignment at $V_g = 0$ and can be tuned by altering the shell thickness. In the absence of confinement, the InAs conduction band edge (CB) lies below the GaSb valence band edge (VB) resulting in a type II-broken band alignment. For thin InAs shells below ≈5–7 nm, however, confinement elevates the lowest electron subband, E1, above VB, and opens a small effective bandgap E_{eff}, yielding a type II-staggered band alignment.[13] In this case (schematically illustrated in Figure 2), an electrostatic gate can be used to tune between electron and hole dominated conduction parallel to the heterointerface. (See Figure S2 in the Supporting Information for a brief overview of relevant band gap configurations.)

In the case of nanowire 1 (NW1), at $V_g = 0$, the Fermi energy E_F is positioned in the effective band gap E_{eff} (Figure 2a). In this configuration both the core and shell are pinched off. The corresponding zero-current plateau can be observed in the conductance measurement of nanowire NW1 at 4.2 K in Figure 2e. If a gate voltage V_g is applied, the bands shift accordingly. At sufficiently large positive gate voltages V_g^+, the lowest electron states in the thin InAs shell are pulled below E_F, and the shell becomes populated with electrons, which gives an increasing conductance with V_g (*n*-type regime in Figure 2c). If a large negative gate voltages V_g^- is applied, the highest hole states of the GaSb are instead pushed above E_F, thus populating the nanowire core with holes. Accordingly, the conductance increases also for decreasing V_g (*p*-type regime in Figure 2c).

If the source contact is heated, as illustrated in Figure 2b, carriers in both channels will diffuse from the hot to the cold side. The resulting open-circuit thermovoltage is displayed in Figure 2d. Similar to the conductance plot in Figure 2c, three different regimes can be distinguished. For $V_g > 2$ V, the thermovoltage is positive, consistent with electron transport (negative charge carriers, see Supporting Information S1). As expected, we observe fluctuations in $V_{Th}(V_g)$ corresponding to the features in $I_D(V_g)$. This fine structure is reproducible between gate sweeps within one cooldown (see Supporting Information Figure S3) and is attributed to 0D-confinement in charge puddles in the InAs shell.[18,34] The magnitude of V_{Th} increases as the Fermi energy approaches the lowest electron states in InAs. The corresponding peak, therefore, distinctively marks the lowest subband position. In the effective band gap regime, between the *p*- and *n*-branches in Figure 2c,d, the thermovoltage exhibits pronounced reproducible fluctuations that reflect the small conductance peaks in this gate voltage interval. Note that the drain-current signal I_D in this regime is generally very small (of the order of pA), and features corresponding to, *e.g.*, quantum-dot resonances can be resolved only poorly due to a small signal-to-noise ratio. The corresponding thermovoltage signal is however very pronounced.

For $V_g < -2.5$ V, the thermovoltage is negative, consistent with hole transport. Both I_D and V_{Th} are smooth compared to the signals in the *n*-branch. This is attributed to the much shorter Fermi wavelength of the holes in GaSb compared to the electrons in the InAs shell (a factor of approximately 20), which leads to a suppression of confinement effects. The GaSb core is also not directly interfacing the HfO_2, which is a source of charge traps for electron transport in the InAs shell, there leading to nonuniform depletion and consequently fluctuations in $G(V_g)$. Nevertheless, a monotonic increase of V_{Th} is observed, as E_F approaches what we interpret as the highest GaSb hole state.

Next, we calculate $V_{Th}(V_g)$ from the measured $G(V_g)$, and compare the results with the $V_{Th}(V_g)$ obtained from electrical measurements. Within a scattering description of transport, S is given by $S = (1/eGT) \int \mathrm{d}E(E - E_F)G(E) \mathrm{d}f(E)/\mathrm{d}E$, where $G(E) = G_h(E) + G_e(E)$, which reduces to the Mott relation in a low-temperature limit. We next divide the measured conductance into two regimes, a hole-dominated and an electron-dominated, with a separation in the middle of the depletion regime. In the electron and hole regimes, we then extract $G(E)$ from $G_e(E) = G(-e\alpha_e V_g)$ and $G_h(E) = G(-e\alpha_h V_g)$, respectively. The lever arm of the gate α relates the applied gate voltage V_g to an absolute energy scale E in the nanowire, $\Delta E = -e\alpha\Delta V_g$. Using the resulting $G(E)$, we can now calculate $S(V_g)$ and compare it with the corresponding experimental measurement, and adapt the used ratio α_e/α_h to match the measured $S(V_g)$. This method works reasonably well when there is a clear depletion regime, such that the conductance can be unambiguously divided into an electron-dominated and a hole-dominated regime.

In Figure 2f, we show $V_{Th} = -S(V_g)\Delta T$ for three different ratios of α_e/α_h, and in Figure 2e, a single curve for $\alpha_e/\alpha_h = 4$, which is the value which best fits the experiment. A reasonable fit can thus only be obtained if we assume that an applied ΔV_g has a smaller effect on hole state energies in the hole regime than on corresponding electron states in the electron regime. Clearly, this method can only give a rough estimate of α_e/α_h, but it reveals important information which could not have been extracted from a conductance measurement alone. In our model we assume that α_e and α_h are constant and do not change with V_g, which yields good results near the band edges where the carrier concentration is moderate. Note that the geometric capacitance based on a simple cylinder-plane model[35] is almost similar for the core and shell. We speculate that the difference in α_e and α_h originates either from energy dependent trap states near the interface of the InAs and the HfO_2 that limit the transconductance in the hole regime, or from a vertical potential gradient induced by the gate voltage that shifts shell states more strongly than core states.[14] In the regime of large V_g, I_D saturates. We attribute this to the increasing relative contribution of series resistance, which leads to significant deviations between modeled and measured thermovoltage. For a more detailed discussion on the effect of series resistance please see Supporting Information S6. Finally, we remark that S is here calculated in linear response, meaning in the limit of vanishing ΔT, and the average temperature is adjusted to achieve a line shape of the same smoothness as the measurement. Therefore, the overall scale in the plots of the calculated $V_{Th} = -S\Delta T$ is arbitrary.

Transport Characterization for Mixed Electron and Hole Transport. When the regimes of electron- and hole transport are not clearly separated, thermovoltage measurements help to identify the point where the dominant charge carrier type switches. At low temperatures, nanowire 2 (NW2) has an $I_D(V_g)$ behavior (Figure 3a,b) similar to that of NW1. The conductance trace exhibits pronounced *p*- and *n*-branches; however, the wire is not completely depleted between the two branches. The overlap of the *p*- and *n*-branches indicates a type II-broken band gap configuration where electrons and holes simultaneously contribute to the electrical transport. We attribute this to a slightly thicker InAs shell in NW2 compared to NW1. In this case, the confinement in the shell is not strong enough to elevate E1 over H1.[13] $V_{Th}(V_g)$ exhibits a distinct sign change at approximately $V_g = 5$ V clearly showing that

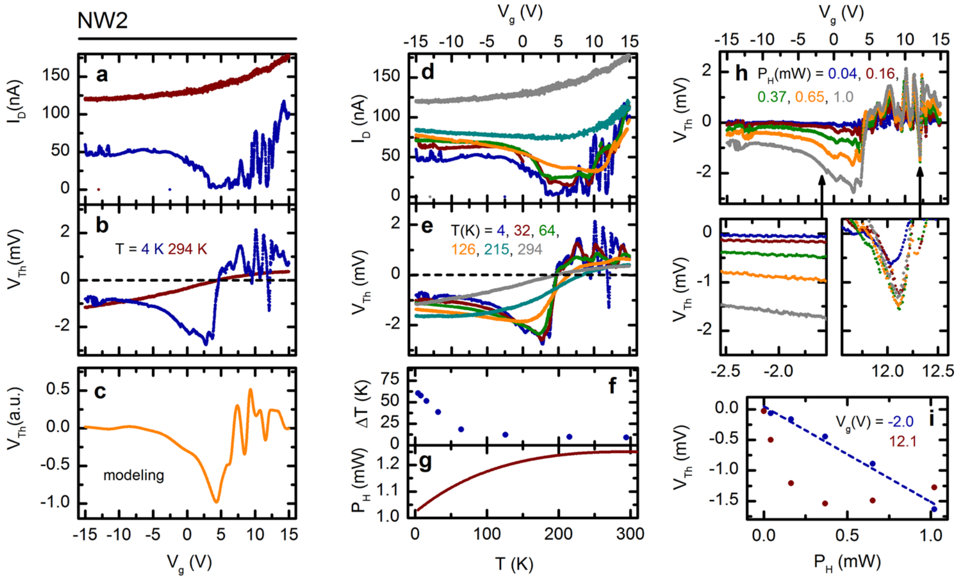

Figure 3. (a) Unlike NW1, NW2 does not exhibit a zero-current plateau in the conductance trace at 4.2 K, indicating a type II-broken band alignment. (b) The thermovoltage shows a clear sign change at around $V_g = 5$ V. Similar to NW1, the modeling (c) based on $G(V_g)$ reproduces the $V_{Th}(V_g)$ well using a α_e/α_h ratio of 4. (d) The ambipolar characteristics of NW2 in the conductance (global minimum) become weaker with rising temperature. However, a clear sign change can still be observed in V_{Th} (e) over the entire temperature range. (f) Rough estimate of the applied temperature difference ΔT across the nanowire segment based on the measurements in ref 28. Note that ΔT increases with decreasing temperature despite the fact that the applied heating power P_H is decreasing (g). (h) V_{Th} for different heating powers (P_H). Note that the thermopower in the smooth region, $V_g < 3$ V, associated with p-type transport in the GaSb core, increases linearly with applied heating power $P_H \propto V_H^2$ (i), whereas the region $V_g > 3$ V, dominated by conductance resonances due to a disordered potential landscape in the n-type InAs, exhibits nonlinear thermovoltage behavior. The applied source-drain bias for (a) and (d) is $V_{SD} = 5$ mV. The heating voltage V_H in (b) and (e) is 0.5 V.

$G_e^T < G_h^T$ for lower gate voltages. Despite the overlap of the p- and n-branches, the thermovoltage trace is well reproduced by the modeling if the separation between the two branches is chosen close to the zero crossing of S at around $V_g = 5$ V.

Temperature Dependence and Additional Information at Room Temperature. Figure 3d,e displays data from conductance and thermovoltage measurements of NW2 that were taken at temperatures T between 4.2 and 294 K. Here, the heating voltage V_H is held constant, whereas the temperature difference ΔT is expected to vary as a function of T. The amplitude of V_{Th} at different T is therefore not immediately comparable. Despite the subsequent reduction in heating power P_H due to the decreasing heater resistance R_H, we expect the temperature difference to increase significantly with decreasing temperature due to a reduction of thermal conductivity of the substrate. A rough estimate of the ΔT and P_H as functions of temperature based on a previous study[28] with similar devices equipped with resistive thermometers is provided in Figure 3f,g.

While at low temperatures the general ambipolar nature of the transport can be deduced, both from the global minimum in $I_D(V_g)$ and the sign change in $V_{Th}(V_g)$, this is not the case at room temperature. Figure 3d shows that with increasing temperature the minimum in the band-region is flooded with thermally excited carriers. At room temperature, $I_D(V_g)$ is fully monotonic leaving no indication of hole transport over the entire gate-voltage range. Such large residual conductance for negative V_g can sometimes be observed for large diameter, and/or highly doped, nanowires where the gate fails to fully deplete the channel. For this nanowire, however, the thermovoltage shows a clear and sharp sign-change indicating the significant contribution of holes to the transport. In fact, for all 6 devices in this study, thermovoltage measurements at room temperature detected the ambipolar nature of the transport, whereas corresponding conductance measurements showed no indication of a p-type contribution for a majority of the devices (see also Supporting Information S4).

Nonlinear Thermovoltage. On the basis of transport signatures in previous studies on bare InAs nanowires,[18,34] we have attributed the sharp peaks in conductance in the n-branch to 0D resonances caused by nonuniform depletion. Next, we investigate nonlinear thermovoltage response with respect to ΔT to obtain additional information about the fine structure in $G(V_g)$. Here, we use the ability of the top-heating device design[28] to apply temperature differentials over a large range of $\Delta T \propto P_H$ of up to tens of Kelvin at a base temperature of 4.2 K.

Figure 3h displays the $V_{Th}(V_g)$ for NW2 for different heating powers at an ambient temperature of 4.2 K. As previously noted, the p-branch has a relatively smooth V_g dependence for all applied heating powers P_H. Despite the application of temperature differences of

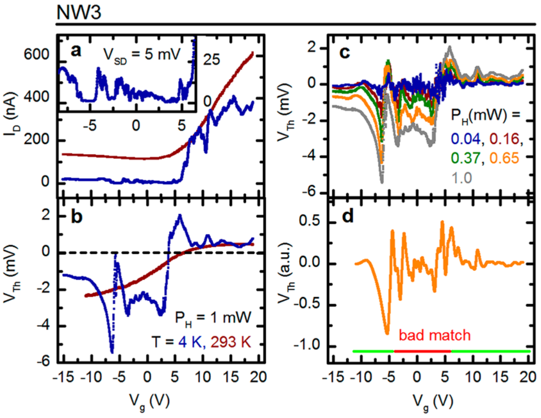

Figure 4. (a) Conductance and (b) thermovoltage measurement of NW3. Similar to NW1, a pronounced zero current plateau associated with type II-staggered band alignment can be observed. Note that the modeling (d) does not match the experimental data in the band gap regime for higher heating powers for any value of α_e/α_h (a ratio of 4 was used in the figure). (c) V_{Th} in this regime shifts rapidly to negative V_{Th} with increased heating power P_H. In this gate voltage interval (approximately between $V_g = -5$ V and $V_g = 5$ V), the conductance exhibits regularly spaced peaks (inset in (a)) that may be attributed to 0D resonances in the InAs shell. The thermovoltage signal (b), however, is overall negative in this regime indicating a contribution of holes in the GaSb.

up to several tens of Kelvins, the *p*-branch thermovoltage increases linearly with the applied heating power (see Figure 3i). In contrast, the peaks in the *n*-branch do not increase linearly with the heating power. The strong fluctuations for all applied P_H including several sign changes of $V_{Th}(V_g)$, *e.g.* around $V_g = 12.1$ V, are characteristic for 0D-like states.[18,36] In fact, for the particular peak at $V_g = 12.1$ V, the thermovoltage increases rapidly with increasing P_H before peaking at approximately P_H = 0.4 mW, and then decreases. This behavior is likely related to thermal broadening of 0D-like resonances, but may also be caused by energy-level renormalization which has previously been observed through thermoelectric measurements on quantum dots.[19]

We now use thermovoltage measurements to extract additional information about the carrier types involved in charge transport in the regime where the *n*- and *p*-branches meet. Figure 4a,b displays data from Nanowire 3 (NW3). Similar to NW1, we observe a pronounced region (approximately between $V_g = -5$ V and $V_g = 5$ V), for which the nanowire is nearly depleted. We attribute the large negative peak of V_{Th} just below $V_g = -6$ V to the first hole-subband edge of the GaSb crossing E_F which is supported by the steep drop in conductance at this gate voltage. We observe an *n*-branch for $V_g > 5$ V signified by an overall positive V_{Th}, an increasing $I_D(V_g)$ and several sharp peaks that we attribute to 0D states in the InAs shell.

A close-up of the near-depletion regime (see inset in Figure 4a) reveals several regularly spaced conductance peaks resembling Coulomb blockade resonances.

From the V_{Th} measurements (Figure 4b,c) we note that, surprisingly, V_{Th} is negative for the whole band gap region identified in the conductance measurements, evidencing a strong hole contribution to the transport.

Figure 4c shows how the thermovoltage evolves with increasing heating power. We find that for small heating powers V_{Th} is dominated by 0D resonances, which in previous studies have been shown to exhibit a high *S* for small ΔT at low *T* due to the sharp energy filtering capacity.[18,36] The larger effective mass of the holes gives a weak confinement, but in turn leads to a larger bulk Seebeck coefficient *S*. At higher heating, their contribution to V_{Th} therefore becomes visible and increases linearly with applied heating power. In the region of interest between $V_g = -5$ V and $V_g = 5$ V, we find moderate oscillations in V_{Th}, but more strikingly a strong overall shift to negative values with increasing heating power. This behavior strongly resembles that of the *p*-branch and leads us to the conclusion that the transport in this regime is dominated by holes. As for the origin of the oscillations in V_{Th} and I_D, we propose that charging of localized/0D states in the InAs shell gives a modulation of the hole transport in the core due to an electrostatic coupling.[37]

We note from Figure 4d that the modeling does not reproduce the measured data in the near-depletion regime since the conductance there cannot unambiguously be attributed to one carrier type. Again we thus find that thermovoltage provides information complementary to conductance, here with relevance to studies of electron–hole interactions.

CONCLUSIONS

We demonstrate that thermovoltage measurements can be an effective tool for characterization of ambipolar nanostructures, both at room temperature and in the quantum transport regime at cryogenic temperatures.

In the investigated GaSb/InAs core–shell nanowires, we find that even in cases where a conductance measurement does not show a clear signature of a hole contribution, a hole dominated regime can reliably be identified using the thermovoltage measurement. This ability to probe the dominating carrier type would also be useful in studies of other ambipolar nanostructures for which standard CV measurements may not be applicable. Examples here are topological insulators, and semiconductor nanostructures that exhibit surface inversion, such as *p*-type InAs nanowires[38] or thick nanowires of a narrow band gap material[39] for which onset of surface inversion will screen depletion of the interior.

In addition, we show that theoretical modeling using the conductance data as input can reproduce the measured thermovoltage under the assumption that electron and hole states shift differently with the applied gate voltage in the regimes of electron and hole conduction. While this method only provides a rough estimate of relative gate lever arms, we foresee that it will be helpful in understanding transport data of various 1D ambipolar devices. It may also be possible to use a single gate to fine-tune the effective band gap in a type-II heterostructure where the electron and hole channels cannot be gated separately, such as in core–shell nanowires.[14,40]

METHODS

Nanowire Growth. GaSb/InAs core–shell nanowires were grown from Au aerosols on a GaAs (111)B substrate using metal organic vapor phase epitaxy (MOVPE; Aixtron 200/4 at 10 kPa in 13 L/min hydrogen carrier). First, Au aerosol particles with a nominal diameter of 30 or 40 nm were dispersed onto the GaAs substrate. After a 7 min annealing step at 630 °C in arsine (AsH_3; molar fraction 1.54e-3), a short GaAs nanowire stem was first grown for 2 min at 450 °C in order to facilitate the nucleation of the GaSb segment, using trimethylgallium (TMGa; molar fraction 3.36×10^{-5}) and AsH_3 (molar fraction 1.23×10^{-3}). GaSb was then grown for 20 min at 530 °C using TMGa (molar fraction 3.36×10^{-5}) and trimethylantimony (TMSb; molar fraction 2.01×10^{-5}). Subsequently, an InAs shell was grown at a temperature of 460 °C using trimethylindium (TMIn, molar fraction 4.53×10^{-6}) and AsH_3 (molar fraction 3.85×10^{-4}) for a duration of 8 min. Previous work has shown that a small amount of Sb is incorporated during the nominal InAs shell growth.[13] For simplicity, however, we refer this material as InAs in this work. Since the nanowires were grown from randomly dispersed Au particles, the axial and radial growth rates vary from wire to wire. From SEM images, where a 10 nm HfO_2 thickness was subtracted from the nanowire radius, it is found that NW1 has a diameter of 75 nm, NW2 of 95 nm, and NW3 of 85 nm. NW4–6 (Supporting Information S4) are thinner, with diameters between 65 and 70 nm. The InAs shell thickness is estimated to be 7 ± 3 nm. The nanowires are nominally undoped, but carbon is known to be incorporated from the precursors during radial overgrowth, which act as *p*-type impurity in GaSb and *n*-type in InAs.

Processing. For this study, only the core–shell segment of the nanowire was contacted. The nanowires were mechanically dry transferred to a highly doped silicon substrate coated with 100 nm of silicon oxide (SiO_2). The electrical contacts to the nanowire were defined using electron-beam lithography (EBL). To remove the native oxide layer, the contacts were etched with diluted buffered HF for 5 s, prior to the contact metal deposition (Ni/Au, 20/120 nm). Following lift-off and a 30 s oxygen plasma etch of polymer residues, the entire device was coated with a 10 nm thick HfO_2 layer *via* atomic layer deposition (ALD) to electrically insulate the heater line from the contacts to the nanowire. In the next step, a focused ion beam (FIB) was employed to mill through the oxide layer above the bond pads designated for the heater line, which was subsequently created in a second EBL step (Ti/Au, 10/140 nm).

Measurements. For the two-probe resistance measurements, a DC source-drain voltage V_{SD} of 5 mV was applied over the nanowire. The resulting drain-current signal I_D was enhanced using a *SR570* low noise current preamplifier (Stanford Research). The thermocurrent I_{Th} was measured in the same constellation under the application of a thermal bias and V_{SD} = 0 mV. I_{Th} was corrected for a small offset current introduced by the current preamplifier. The highly doped Si substrate with a 100 nm SiO_2 layer was used as a back gate.

To induce a temperature difference across the nanowire, a heating voltage V_H was applied over the heater circuit. The resulting heating current I_H is determined by R_H and a serial resistor $R_S = 50\ \Omega$, $I_H = V_H/(R_H + 50\ \Omega)$. The heating power P_H is then given by $P_H = I_H^2 R_H$, where R_H is of the order of 20 Ω at 4.2 K. The positioning of the heater on top of the electrical contact to the nanowire allows for the application of large thermal biases. On the basis of measurements on similar devices[28] equipped with resistive thermometers, the applied temperature difference ΔT per mW is estimated to be of the order of 60 K/mW at 4.2 K where $\Delta T \propto P_H$ while the temperature rise of the cold contact remains below the resolution of the applied resistive thermometer method (please see ref 28 for a detailed study of the heating method).

The induced thermovoltage V_{Th} was probed using a femto (DLPVA-100-F-D) voltage preamplifier with 1 TΩ input impedance. V_{Th} was corrected for a constant offset that was measured at V_H = 0 mV to ensure all contributions of voltage buildups in the system and instrument offsets were eliminated. All measurements where performed in a helium dewar with a sample holder that was equipped with a LakeShore Si diode temperature sensor.

Conflict of Interest: The authors declare no competing financial interest.

Acknowledgment. This work was supported by the Swedish Energy Agency (Grant No. P38331-1), the Nanometer Structure Consortium at Lund University (nmC@LU), the Swedish Research Council (VR), the Swedish Foundation for Strategic Research (SSF), and the Knut and Alice Wallenberg Foundation (KAW). C.T. and H.L. conceived the study. B.G., C.T., and K.A.D. contributed to the nanowire development, J.G.G. and C.T. designed and fabricated the devices and J.G.G. carried out the measurements. M.L. carried out the theoretical modeling. J.G.G., C.T., M.L., and H.L. analyzed the data, and all authors contributed to writing the manuscript.

Supporting Information Available: A brief overview of the possible band-alignment configurations, additional data supporting the reproducibility and consistency of our results and a brief discussion of the origin of the Seebeck coefficient and the impact of possible series resistance due to the axial InAs segment. The Supporting Information is available free of charge on the ACS Publications website at DOI: 10.1021/acsnano.5b01495.

REFERENCES AND NOTES

1. Sakaki, H.; Chang, L. L.; Ludeke, R.; Chang, C.-A.; Sai-Halasz, G. A.; Esaki, L. $In_{1-x}Ga_xAs$-$GaSb_{1-y}As_y$ Heterojunctions by Molecular Beam Epitaxy. *Appl. Phys. Lett.* **1977**, *31*, 211–213.
2. Kroemer, H. The 6.1 Å Family (InAs, GaSb, AlSb) and Its Heterostructures: A Selective Review. *Physica E* **2004**, *20*, 196–203.
3. Pawlik, D.; Romanczyk, B.; Thomas, P.; Rommel, S.; Edirisooriya, M.; Contreras-Guerrero, R.; Droopad, R.; Loh, W.-Y.; Wong, M. H.; Majumdar, K.; et al. Benchmarking and Improving III-V Esaki Diode Performance with a Record 2.2 MA/cm^2 Peak Current Density to Enhance TFET Drive Current. *IEEE Int. Electron Devices Meet.* **2012**, 27.1.1–27.1.3.
4. Borg, B. M.; Ek, M.; Ganjipour, B.; Dey, A. W.; Dick, K. A.; Wernersson, L.-E.; Thelander, C. Influence of Doping on the Electronic Transport in GaSb/InAs(Sb) Nanowire Tunnel Devices. *Appl. Phys. Lett.* **2012**, *101*, No. 043508.
5. Zhou, G.; Li, R.; Vasen, T.; Qi, M.; Chae, S.; Lu, Y.; Zhang, Q.; Zhu, H.; Kuo, J.-M.; Kosel, T.; et al. Novel Gate-Recessed Vertical InAs/GaSb TFETs with Record High I_{ON} of 180 μA/μm at V_{DS} = 0.5 V. *IEEE Int. Electron Devices Meet.* **2012**, 32.6.1–32.6.4.
6. Ganjipour, B.; Dey, A. W.; Borg, B. M.; Ek, M.; Pistol, M.-E.; Dick, K. A.; Wernersson, L.-E.; Thelander, C. High Current Density Esaki Tunnel Diodes Based on GaSb–InAsSb Heterostructure Nanowires. *Nano Lett.* **2011**, *11*, 4222–4226.

7. Sai-Halasz, G. A.; Esaki, L.; Harrison, W. A. InAs-GaSb Superlattice Energy Structure and Its Semiconductor-Semimetal Transition. *Phys. Rev. B* **1978**, *18*, 2812–2818.
8. Fuchs, F.; Weimer, U.; Pletschen, W.; Schmitz, J.; Ahlswede, E.; Walther, M.; Wagner, J.; Koidl, P. High Performance InAs/Ga$_{1-x}$In$_x$Sb Superlattice Infrared Photodiodes. *Appl. Phys. Lett.* **1997**, *71*, 3251–3253.
9. Suzuki, K.; Harada, Y.; Onomitsu, K.; Muraki, K. Edge Channel Transport in the InAs/GaSb Topological Insulating Phase. *Phys. Rev. B* **2013**, *87*, No. 235311.
10. Knez, I.; Du, R.-R.; Sullivan, G. Evidence for Helical Edge Modes in Inverted InAs/GaSb Quantum Wells. *Phys. Rev. Lett.* **2011**, *107*, No. 136603.
11. Ek, M.; Borg, B. M.; Dey, A. W.; Ganjipour, B.; Thelander, C.; Wernersson, L.-E.; Dick, K. A. Formation of the Axial Heterojunction in GaSb/InAs(Sb) Nanowires with High Crystal Quality. *Cryst. Growth Des.* **2011**, *11*, 4588–4593.
12. Borg, B. M.; Dick, K. A.; Ganjipour, B.; Pistol, M.-E.; Wernersson, L.-E.; Thelander, C. InAs/GaSb Heterostructure Nanowires for Tunnel Field-Effect Transistors. *Nano Lett.* **2010**, *10*, 4080–4085.
13. Ganjipour, B.; Ek, M.; Borg, B. M.; Dick, K. A.; Pistol, M.-E.; Wernersson, L.-E.; Thelander, C. Carrier Control and Transport Modulation in GaSb/InAsSb Core/Shell Nanowires. *Appl. Phys. Lett.* **2012**, *101*, No. 103501.
14. Qu, F.; Beukman, A. J. A.; Nadj-Perge, S.; Wimmer, M.; Nguyen, B.-M.; Yi, W.; Thorp, J.; Sokolich, M.; Kiselev, A. A.; Manfra, M. J.; et al. Electric and Magnetic Tuning between the Trivial and Topological Phases in InAs/GaSb Double Quantum Wells. **2015**, *arXiv:1502.05714 [cond-mat.mes-hall]*.
15. Roddaro, S.; Ercolani, D.; Safeen, M. A.; Suomalainen, S.; Rossella, F.; Giazotto, F.; Sorba, L.; Beltram, F. Giant Thermovoltage in Single InAs Nanowire Field-Effect Transistors. *Nano Lett.* **2013**, *13*, 3638–3642.
16. Schmidt, V.; Mensch, P. F. J.; Karg, S. F.; Gotsmann, B.; Das Kanungo, P.; Schmid, H.; Riel, H. Using the Seebeck Coefficient to Determine Charge Carrier Concentration, Mobility, and Relaxation Time in InAs Nanowires. *Appl. Phys. Lett.* **2014**, *104*, No. 012113.
17. Seol, J. H.; Moore, A. L.; Saha, S. K.; Zhou, F.; Shi, L.; Ye, Q. L.; Scheffler, R.; Mingo, N.; Yamada, T. Measurement and Analysis of Thermopower and Electrical Conductivity of an Indium Antimonide Nanowire from a Vapor-Liquid-Solid Method. *J. Appl. Phys.* **2007**, *101*, No. 023706.
18. Wu, P. M.; Gooth, J.; Zianni, X.; Svensson, S. F.; Gluschke, J. G.; Dick, K. A.; Thelander, C.; Nielsch, K.; Linke, H. Large Thermoelectric Power Factor Enhancement Observed in InAs Nanowires. *Nano Lett.* **2013**, *13*, 4080–4086.
19. Fahlvik Svensson, S.; Hoffmann, E. A.; Nakpathomkun, N.; Wu, P. M.; Xu, H. Q.; Nilsson, H. A.; Sánchez, D.; Kashcheyevs, V.; Linke, H. Nonlinear Thermovoltage and Thermocurrent in Quantum Dots. *New J. Phys.* **2013**, *15*, No. 105011.
20. Matthews, J.; Battista, F.; Sánchez, D.; Samuelsson, P.; Linke, H. Experimental Verification of Reciprocity Relations in Quantum Thermoelectric Transport. *Phys. Rev. B* **2014**, *90*, No. 165428.
21. Scheibner, R.; König, M.; Reuter, D.; Wieck, A. D.; Gould, C.; Buhmann, H.; Molenkamp, L. W. Quantum Dot as Thermal Rectifier. *New J. Phys.* **2008**, *10*, No. 083016.
22. Matthews, J.; Sánchez, D.; Larsson, M.; Linke, H. Thermally Driven Ballistic Rectifier. *Phys. Rev. B* **2012**, *85*, No. 205309.
23. Thierschmann, H.; Henke, M.; Knorr, J.; Maier, L.; Heyn, C.; Hansen, W.; Buhmann, H.; Molenkamp, L. W. Diffusion Thermopower of a Serial Double Quantum Dot. *New J. Phys.* **2013**, *15*, No. 123010.
24. Tian, Y.; Sakr, M. R.; Kinder, J. M.; Liang, D.; MacDonald, M. J.; Qiu, R. L. J.; Gao, H.-J.; Gao, X. P. A. One-Dimensional Quantum Confinement Effect Modulated Thermoelectric Properties in InAs Nanowires. *Nano Lett.* **2012**, *12*, 6492–6497.
25. Dzurak, A. S.; Smith, C. G.; Barnes, C. H. W.; Pepper, M.; Martín-Moreno, L.; Liang, C. T.; Ritchie, D. A.; Jones, G. A. C. Thermoelectric Signature of the Excitation Spectrum of a Quantum Dot. *Phys. Rev. B* **1997**, *55*, R10197–R10200.
26. Nolas, G. S.; Sharp, J.; Goldsmid, J. *Thermoelectrics: Basic Principles and New Materials Developments*; Springer Science & Business Media: New York, 2001; p 38.
27. Dey, A. W.; Svensson, J.; Ek, M.; Lind, E.; Thelander, C.; Wernersson, L.-E. Combining Axial and Radial Nanowire Heterostructures: Radial Esaki Diodes and Tunnel Field-Effect Transistors. *Nano Lett.* **2013**, *13*, 5919–5924.
28. Gluschke, J. G.; Svensson, S. F.; Thelander, C.; Linke, H. Fully Tunable, Non-Invasive Thermal Biasing of Gated Nanostructures Suitable for Low-Temperature Studies. *Nanotechnology* **2014**, *25*, No. 385704.
29. Sivan, U.; Imry, Y. Multichannel Landauer Formula for Thermoelectric Transport with Application to Thermopower Near the Mobility Edge. *Phys. Rev. B* **1986**, *33*, 551–558.
30. Mahan, G. D.; Sofo, J. O. The Best Thermoelectric. *Proc. Natl. Acad. Sci. U.S.A.* **1996**, *93*, 7436–7439.
31. Mahan, G. D. DC Conductivities. In *Many-Particle Physics*; Physics of Solids and Liquids; Springer: New York, 2000; pp 499−577.
32. Kim, D.; Syers, P.; Butch, N. P.; Paglione, J.; Fuhrer, M. S. Ambipolar Surface State Thermoelectric Power of Topological Insulator Bi$_2$Se$_3$. *Nano Lett.* **2014**, *14*, 1701–1706.
33. Lunde, A. M.; Flensberg, K. On the Mott Formula for the Thermopower of Non-Interacting Electrons in Quantum Point Contacts. *J. Phys.: Condens. Matter* **2005**, *17*, 3879–3884.
34. Weis, K.; Wirths, S.; Winden, A.; Sladek, K.; Hardtdegen, H.; Lüth, H.; Grützmacher, D.; Schäpers, T. Quantum Dots in InAs Nanowires Induced by Surface Potential Fluctuations. *Nanotechnology* **2014**, *25*, No. 135203.
35. Ramo, S.; Whinnery, J. R.; van Duzer, T. *Fields and Waves in Communication Electronics*, 3rd ed.; Wiley: New York, 1993; p 345.
36. Fahlvik Svensson, S.; Persson, A. I.; Hoffmann, E. A.; Nakpathomkun, N.; Nilsson, H. A.; Xu, H. Q.; Samuelson, L.; Linke, H. Lineshape of the Thermopower of Quantum Dots. *New J. Phys.* **2012**, *14*, No. 033041.
37. Ganjipour, B.; Leijnse, M.; Samuelson, L.; Xu, H. Q.; Thelander, C. Transport Studies of Electron-Hole and Spin-Orbit Interaction in GaSb/InAsSb Core-Shell Nanowire Quantum Dots. *Phys. Rev. B* **2015**, *91*, No. 161301.
38. Upadhyay, S.; Jespersen, T. S.; Madsen, M. H.; Krogstrup, P.; Nygård, J. Low Temperature Transport in p-Doped InAs Nanowires. *Appl. Phys. Lett.* **2013**, *103*, No. 162104.
39. Karlström, O.; Wacker, A.; Nilsson, K.; Astromskas, G.; Roddaro, S.; Samuelson, L.; Wernersson, L.-E. Analysing the Capacitance−Voltage Measurements of Vertical Wrapped-Gated Nanowires. *Nanotechnology* **2008**, *19*, No. 435201.
40. Naveh, Y.; Laikhtman, B. Band-Structure Tailoring by Electric Field in a Weakly Coupled Electron-Hole System. *Appl. Phys. Lett.* **1995**, *66*, 1980–1982.